



**HAL**  
open science

## Fracture Characterization and Stochastic Modeling of the Granitic Basement in the HDR Soultz Project (France)

Benoît Massart, Marie Paillet, Vincent Henrion, Judith Sausse, Chrystel  
Dezayes, Albert Genter, Adrien Bisset

► **To cite this version:**

Benoît Massart, Marie Paillet, Vincent Henrion, Judith Sausse, Chrystel Dezayes, et al.. Fracture Characterization and Stochastic Modeling of the Granitic Basement in the HDR Soultz Project (France). World Geothermal Congress 2010, Apr 2010, Bali, Indonesia. 7 p. hal-00496923

**HAL Id: hal-00496923**

**<https://brgm.hal.science/hal-00496923>**

Submitted on 1 Jul 2010

**HAL** is a multi-disciplinary open access archive for the deposit and dissemination of scientific research documents, whether they are published or not. The documents may come from teaching and research institutions in France or abroad, or from public or private research centers.

L'archive ouverte pluridisciplinaire **HAL**, est destinée au dépôt et à la diffusion de documents scientifiques de niveau recherche, publiés ou non, émanant des établissements d'enseignement et de recherche français ou étrangers, des laboratoires publics ou privés.

## Fracture Characterization and Stochastic Modeling of the Granitic Basement in the HDR Soutz Project (France)

Benoît Massart<sup>1</sup>, Marie Paillet<sup>1</sup>, Vincent Henrion<sup>1</sup>, Judith Sausse<sup>2</sup>, Chrystel Dezayes<sup>3</sup>, Albert Genter<sup>4</sup>, Adrien Bisset<sup>5</sup>

<sup>1</sup> CRPG-CNRS, ENSG, Nancy Université, rue du doyen Marcel Roubault, BP 40, 54501 Vandoeuvre-lès-Nancy, France

<sup>2</sup> Nancy Université, Département des Sciences de la Terre, UMR CNRS 7566 G2R, BP239, 54506 Vandoeuvre les Nancy, France.

<sup>3</sup> Département Géothermie, BRGM, 3, avenue C. Guillemin - BP 6009 - 45060 Orléans Cedex 2, France

<sup>4</sup> EEIG Exploitation Minière de la Chaleur, Route de Soutz, BP38, F-67250 Kutzenhausen, France

<sup>5</sup> BeicipFranlab, 232, Av. Napoléon Bonaparte, 92502 Rueil-Malmaison, France

**Keywords:** Fractures, Faults, Statistics, Soutz, Damage zone, Fractal dimension, Discrete Fracture Networks

### ABSTRACT

The quantification and modeling of fluid flow in fractured rocks are extensively studied to solve and predict numerous economic or environmental problems (hydrothermalism, geothermy, storages, etc.). Indeed, discontinuities such as faults and fractures are potential sites for fluid circulation and have important implications for the hydraulic properties of rocks. The matrix permeability of igneous rocks is generally small and, consequently, the global permeability is mostly controlled by the fault and fracture networks. Therefore, the quantification of the fractured rock hydraulic properties strongly depends on the knowledge of the geometrical parameters of fractures (orientation, extension, aperture, density) and of the final 3D modeling of the fracture network organization.

In the specific case of the Soutz-Sous-Forêts geothermal reservoir, a new statistical analysis of the fault and fracture networks is proposed to precise the actual 3D structural model of the reservoir (Sausse et al., 2009; Dezayes et al., 2009). The statistical characterization of the fractures and faults is realized with the re-interpretation of the whole U.B.I. images database available at Soutz. 1800 fractures are determined along the three deep Soutz well paths, grouped into main conjugates fractures sets, showing a mean N-S orientation and a mean dip of 70°, consistent with the Oligocene N-S extension responsible of the formation of the French Rhine graben. A correlation between the geometric parameters of fractures, width  $W$  and extension  $L$  is proposed and follows a power-law type correlation of the form  $L = k \cdot W^D$  with  $k$ , a coefficient characteristic of the facies and  $D$  the fractal dimension of the fracture set. These parameters are used to determine the volumetric density of fractures (number of fractures/m<sup>3</sup>) at the wells scale. Finally, this density and the statistics of fracture properties are used to constrain stochastic simulation of a discrete fracture network (DFN) in the geothermal reservoir.

### 1. INTRODUCTION

The geothermal reservoir of Soutz-Sous-Forêts is a naturally fractured granitic basement, located in the Rhine graben in Alsace, France, where a thermal anomaly of around 200°C is observed at a depth of 5000 m. This high temperature at depth and the location of other oil-producing wells in the historic Pechelbronn field region, which provide many informations concerning the geology of the basin, are the reasons of the implantation of the European Soutz experimental geothermal pilot plant since 1987. High

pressured water is injected in this non-porous but fractured media in order to stimulate the natural existing fractures in the rock by hydraulic fracturation. It leads to an enhancement of the fracture permeability and connectivity between the injection and production wells and within the reservoir. Cold water is injected in a central well and is produced after heating up at depth by two other lateral wells that constitute the geothermal triplet.

In this case, the fracture network mainly controls the hydraulic behavior of the reservoir and the characterization of the fractures is then crucial for the study of flows and for production optimization. This analysis is reliable at the well scale where Ultra Sonic Borehole Images (U.B.I.) data are available but a large incertitude appears at the reservoir scale far from the wells. Moreover, in the case of basement fractured rock such as Soutz, fractures and faults represent complex and composite structures. A Fault zone is characterized by a large damage zone where intense microfracturing and alteration could be observed (Genter et al. 2000). These complex fault zones constitute the main drains of the reservoir.

This paper reports a new statistical interpretation of the fracture and faults at Soutz. The characterization of the main fracture sets allow the modeling of a DFN (Discrete Fracture Network) in the reservoir and the modeling of the derived hydraulic properties that are compared to the results of the numerous flow tests that were realized at Soutz. This paper focuses on the different steps of the statistical analysis and the determination of the fractures set parameters. Then, the chosen criteria that constrain the DFN simulation are proposed. The objective of such study is to construct consistent DFN model which can be used as a basis for flow study.

### 2. GEOLOGICAL DATA: ACQUISITION AND PROCESSING

Soutz-Sous-Forêts, located in the Upper Rhine Graben, hosts one of the few deep geothermal 'Enhanced Geothermal System' test sites in the world. At its current state of development (Gérard et al. 2006), the EGS site consists of six boreholes. GPK2, GPK3 and GPK4 constitute the European geothermal pilot plant which extends to more than 5000 m depth, GPK1 a first hydraulic test well which extends to 3600 m and a reference hole EPS1 which has been fully cored down to 2230 m. Some seismic observation wells are located near from the geothermal plant. Well 4550 is the closest from the wellhead of GPK1 (Figure 1A).

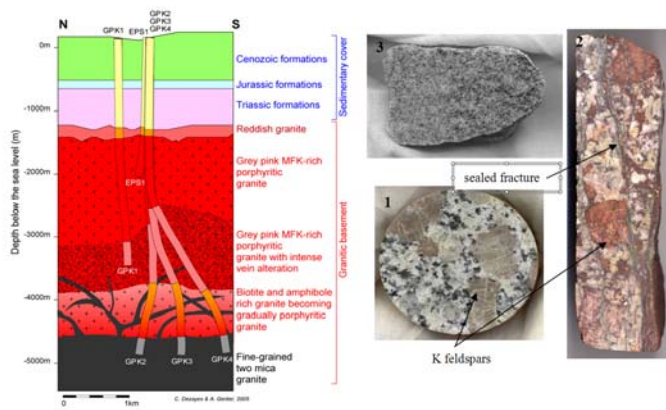


**Figure 1: A. Lithological schematic cross-section of the Soultz site (Dezayes et al. 2005). B. Picture 1 : plug of the fresh porphyritic granite facies (well GPK1(K5-20)); Picture 2 : strongly altered porphyritic granite facies, one sealed fracture could be observed (well GPK1, K21, 3510 m); Picture 3 : Two-micas granite facies (well GPK2, K1, 5058.30 m).**

The French Geological Survey (BRGM) collected geological and well logging data to characterize the Soultz fractured granite reservoir in terms of petrography, hydrothermal alteration and natural fracture network; well data were acquired by logging companies. Numerous hydraulic stimulations of the deep wells generated micro-seismic activity which was interpreted in terms of major structures in order to try to relate events location with fault organisation (Dorbath et al, in press). Numerous hydraulic data such as flow logs are too available (Nami et al., 2008, Schindler et al., 2008).

**2.1. Facies of the Soultz granite reservoir**

The Soultz basement is represented by two different facies. A first monzogranite facies is observed under Triassic to actual sedimentary deposits, at 1200 m depth and consists of porphyritic granite, rich in potassic feldspars appearing in a quartz, plagioclase, biotite and amphibole matrix. This first facies could be locally strongly altered (Genter 1989) (Figure 1.B. Picture 1). The intense alteration is due to a succession of hydrothermal events of three types:

- a generalized and pervasive alteration of the matrix by formation water flows;
- an illitization localized in the fractures zones, which matches with high Gamma-Ray signatures on well geophysical logs. This alteration leads to the sealing of the majority of natural fractures (no permeability) (Figure 1.B. Picture 2);
- a rubefaction of the top of the granite due to its emersion and its alteration by surface waters.

The second facies, crosscut by the wells at high depth (> 4000 m), is a two micas facies, composed of biotite and muscovite in a grey quartz matrix. The facies is more homogeneous and less concerned by the hydraulic alteration than the upper one (Dezayes et al. 2005) (Figure 1B, Picture 3).

**2.2. Faults and associated damage zone**

In the case of the Soultz reservoir modeling, a particular attention was paid to the modeling of the faults. Dezayes et al. (2009) and Sausse et al. (2009) recently proposed a new

3D model of the fault networks based on high quality datasets such as geological data, well logs, microseismicity recordings during hydraulic stimulations of the wells and vertical seismic profiling (V.S.P.). One major fault is identified in GPK1, GPK2 and GPK3 where it concentrates the majority of the fluid losses during flow tests (75 % of fluid loss). This major fault represents a complex clustered structure when observed at well scale and appears with a large damage zone on U.B.I. images. A damage zone consists of a volume of deformed rocks around a fault surface that results from the initiation, propagation, interaction and build-up of slip along faults (Kim et al. 2004). The resulting displacements are balanced by the opening of conjugate fractures along the fault plane. The damage zone becomes larger and larger with the fault growth. The first initial fractures grow in the same time and generate fractures in their turn to balance their opening. Genter et al. (2000) proposed a damage zone model of the fracture zones observed at Soultz. Three zones could be identified from the fault core to its periphery (Figure 2):

1. The fault core is the less porous part of the damage zone. In this example, it is mainly sealed by secondary quartz crystallization.
2. The cataclased and brecciated zones are more or less obstructed by fine particles, shales or silts, which are generated by the shear along the fault.
3. The hydrothermally altered zones are high porosity zones where fluids flows could be concentrated.

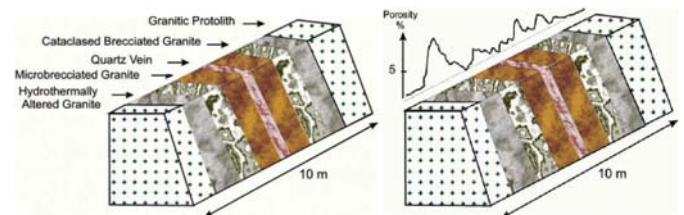


**Figure 2: Conceptual lithofacies granite zonation and porosity profile of a hydrothermally altered and fractured zone at Soultz (Genter et al. 2000).**

The major fault observed in GPK3 generates a damage zone of around 13 m wide along the well path.

**3. STATISTICAL ANALYSIS OF ULTRASONIC BOREHOLE IMAGES (U.B.I.)**

**3.1. Ultrasonic borehole imagery (U.B.I.) and fracture identification**

GPK2, GPK3 and GPK4 wells were logged with U.B.I. tools. These acoustic tools record amplitude and transit time data of acoustic waves reflected by the borehole walls and therefore allow the determination of contrast of sonic velocities that reveals facies variations of fracture zones (Figure 3A).

Centimetric fractures could be detected thanks to the accurate U.B.I. vertical resolution of 0.5 to 1 cm. However the sonic wave lateral penetration is quite low, with a sampling interval of 0.1 inch (2.54 mm).

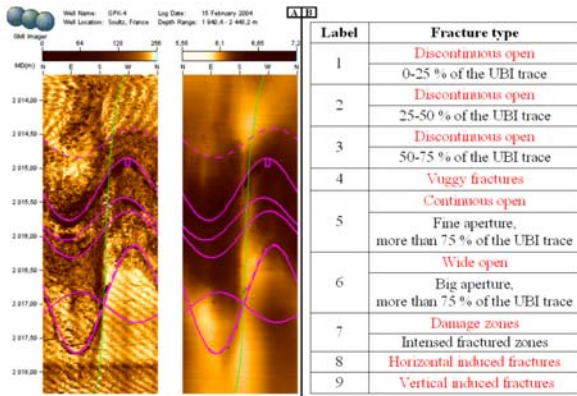


**Figure 3: A. Examples of fracture and damage zone identifications on U.B.I. images. The pink sinusoidal curves correspond to fractures traces corresponding to contrasted amplitudes (left U.B.I. image) and transit times (right U.B.I. image). An open fracture is characterized by both amplitude and transit time traces. The dotted curves mark the boundaries of a damage zone. The true dip and dip direction of the fractures are derived from the sinusoidal curve characteristics. B. Picking and classification of the fractures.**

This work focuses only on open fractures that host fluid flows in the reservoir. However, the real effective opening of a fracture remains difficult to define. Closed fractures are sealed by secondary re-crystallization or filled with fine impermeable particles (only amplitude traces on U.B.I.). The main faults present damage zone and largely open fractures (both amplitude and transit time traces on U.B.I.). Between these two extreme opening states, several other types of fracture width are proposed in this study (Figure 3B).

A total of 1878 open fractures were located on GPK2, GPK3 and GPK4 UBI logs (Figure 3.B.), amongst which 1637 were defined as natural open fractures (labels 1 to 6) , 82 were defined as damage zones (label 7) and 159 were defined as horizontal induced drilling fractures (label 8). For

each fracture, its measured depth, true dip, dip direction, and aperture (continuous or fragmented sinusoids) are recorded.

Previous other main fracture zones (Sausse et al., 2009; Dezayes et al., 2009) are characterized by labels 11 to 14.

### 3.2 Statistical analysis of fractures versus labels, orientations and facies

Table 1 presents the main results of the fracture database statistical analysis.

For the three deep wells GPK2, GPK3 and GPK4, fractures are organized in two main orientation sets showing a mean North-South direction and East or West dips forming conjugated sets coherent with the direction of the Rhine Graben opening. Statistical analysis were therefore performed for each orientation sets: 'Fracture set W.' corresponding to the West dipping fractures and 'Fracture set E.' to the East dipping ones. The Fisher coefficient was determined for each set. This parameter is equivalent to the standard deviation parameter in the case of spherical geometry space such as orientation data. Low values indicate a high dispersion of orientations within a set and at the opposite, high values of the Fisher coefficient indicate homogeneous or well distributed orientations. The Fisher coefficients range from 0.6 to 10.68 in this case. The same order of magnitudes is observed for the sets W. and E. with lower dispersion for the dips than for the dip directions (Table 1.B and 1.C).

The linear fracture density is calculated using the ratio between the number of fractures observed on U.B.I. logs and the total logged length of the well path. The global fracture density (Sets W. and E.) is equal to 1.890 fractures/m in the facies 1 and a lower value of 0.952 fractures/m is observed in facies 2. This difference could be explained by different mechanical behaviors of the granitic facies and therefore types of fracturing. The two micas facies could have a more plastic behavior due to the high presence of anisotropic micas.

A		Number of fractures	rate (%)	Number of fractures FACIES 1	Number of fractures FACIES 2	Number of fractures SET W	Number of fractures SET E
1	Discontinuous open traces (25%)	1361	72.47	1170	191	837	524
2	Discontinuous open traces (50%)	85	4.53	83	2	47	38
3	Discontinuous open traces (75%)	30	1.60	21	9	16	14
4	Vuggy Fractures	125	6.84	117	8	86	39
5	Continuous open	23	1.22	20	3	17	6
6	Wide open	13	0.69	10	3	8	5
7	Damage zones	82	4.37	80	2	49	33
8	Induced subhorizontal drilling fractures	159	8.47	137	22	88	71
<b>Total</b>		<b>1878</b>	<b>100</b>	<b>1638</b>	<b>240</b>	<b>1148</b>	<b>730</b>
<b>Fracture density (Fractures/m)</b>				<b>1.890</b>	<b>0.952</b>	<b>0.18</b>	<b>0.12</b>

B		SET W			
Label & fracture type	Mean Dip Direction	Fisher coefficient	Mean Dip	Fisher coefficient	Fracture density (Fractures/m)
1 Discontinuous open traces (25%)	263	0.73	68	5.8	0.202
2 Discontinuous open traces (50%)	249	0.92	67	5.65	0.177
3 Discontinuous open traces (75%)	246	1.3	61	3.74	0.003
4 Vuggy Fractures	270	0.6	63	4.77	0.017
5 Continuous open	247	1.29	72	8.24	0.006
6 Wide open	241	1.14	58	10.68	0.002
<b>All fractures</b>	<b>266</b>	<b>0.72</b>	<b>68</b>	<b>5.57</b>	<b>0.18</b>

C		SET E			
Label & fracture type	Mean Dip Direction	Fisher coefficient	Mean Dip	Fisher coefficient	Fracture density (Fractures/m)
1 Discontinuous open traces (25%)	81	1.1	69	5.57	0.134
2 Discontinuous open traces (50%)	77	1	74	10.07	0.012
3 Discontinuous open traces (75%)	96	1.23	70	6.87	0.004
4 Vuggy Fractures	74	1.17	71	7.32	0.011
5 Continuous open	76	3.89	71	10.68	0.002
6 Wide open	117	1	71	2.71	0.002
<b>All fractures</b>	<b>77</b>	<b>1.06</b>	<b>70</b>	<b>5.65</b>	<b>0.12</b>

**Table 1: main results of the fracture database statistical analysis. A. The number of fractures, their relative proportion is presented by facies and by sets of orientations. B & C The mean dip directions, dips and the linear density along the well paths are mentioned for the two main sets presented by label and West (B) and East dips (C).**



Discontinuous open fractures are the most numerous: labels 1, 2 and 3 represent 78.6 % of the whole fracture database. This fracture type is more represented in the second facies, two-micas granite, than in the first one, porphyritic granite. As a general manner, the two mica granite shows less alteration and less numerous fractures than the porphyritic granite. Only few vuggy, continuous and wide open fractures are observed (8.5 % of the whole database). These fractures that represent main drains in the reservoir stays isolated an match with the biggest structures described by Dezayes et al. (2009) and Sausse et al. (2009).

The conjugated sets are not distributed homogeneously with depth. The first facies hosts a higher rate of West dipping fractures (60 %) than East dipping fractures (40 %). The bottom part of the reservoir in the second facies shows a majority of West dipping fractures (80 %). The in-situ stress tensor and the resulting fracture orientations at depth could be modified due to the presence of big faults of the Rhine graben (Dezayes et al. 2009).

### 3.3. Statistical analysis of fracture sizes and widths

A D.F.N. (Discrete Fracture Network) modeling of the fractured reservoir requires the definition of a volume of interest (V.O.I.) around the reservoir wells that is represented by a regular grid containing voxels characterized by a volumetric fracture density property. The fracture database is acquired at the well scale. However, the major issue for reconstructing the 3D geometry of the Soultz fracture network is the question of the fracture extensions.

According to Johnston (1996), the extension of a fracture is linked to its width by :

$$L = k \cdot W^D \tag{1}$$

where  $L$  is the extension of the fracture,  $W$  its width,  $k$  a coefficient characteristic of the facies and  $D$  the fractal dimension of the fracture set.

#### 3.3.1 Fractal dimension of the fracture network

Mandelbrot (1984) defines a fractal object as being a rough or fragmented geometric shape that can be split into identical parts whatever the scale of observation. This property is called self-similarity. Each elementary shapes is (at least approximately) a reduced-size copy of the whole shape and has a probability of occurrence  $P$  that is related to the fractal dimension  $D$ , by the relation :

$$P = x^{-D} \tag{2}$$

where  $x$  is a characteristic length of the shape, that could be the extension of the fracture or its width. The fractal dimension  $D$  is a decimal number that ranges from 1 to 2 in the case of 2-D. studies. Low  $D$  indicates clustered events while high  $D$  corresponds to more regularly spaced ones.

Two approaches were undertaken to determine the fractal dimension of the Soultz fracture network. All of these approaches are described precisely in Bonnet et al. (2001):

- The first approach uses the frequency distribution of the fracture width.
- The second one is the spacing interval method (Harris et al. 1991).

### Frequency distribution of the fracture geometry: Number of fractures versus mean width per label

The new fracture database presented in this paper includes all fracture types, faults and damage zones observed in the wells GPK2, GPK3 and GPK4 and are analyzed using the relation between fracture occurrences (probability of fracture intersection with the wells) and widths such as proposed by Bonnet et al. (2001). The damage zones do not represent strictly fractures, but their vertical extension along the wells was assimilated to the width of the associated faults previously defined by Dezayes et al. (2009) and Sausse et al. (2009). For example, the major fault that intercepts the well GPK3 at 4775 m (M.D.) is surrounded by a damage zone of 13 m. This fault is therefore characterized by a 13 m width equal to its damage zone width in the database. In Figure 4 is presented a bi-logarithm diagram that plots the number of fractures  $n$  of each label as a function of their mean width  $W$ . White dots in Figure 4 correspond to the fracture labels that are correlated over a large magnitude of fracture widths. In black are plot "problematic" points, corresponding to fracture labels 5 and 6. This relation is well fit ( $R^2=0.9665$ ) to a power law equation with an exponent equal to 1.04.

A	Label & fracture type	Mean widths $W$ (cm)	Number of fractures
1	Discontinuous open traces (25%)	3.15	1476
2	Discontinuous open traces (50%)		
3	Discontinuous open traces (75%)		
4	Vuggy Fractures	10.69	125
5	Continuous open fractures	6.32	23
6	Wide open fractures	20.31	13
11	minor faults	150.11	18
12	medium faults	269.83	8
14	major faults	626.53	4

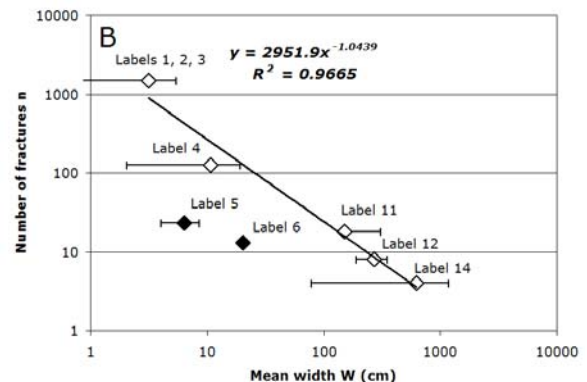


**Figure 4:** A. Bi-logarithm diagram representing the number of fractures  $n$  as a function of their width  $W$  in cm. B. Data used for the plot for each fracture label. The values into brackets correspond to extrapolated data, proportional to the number of fractures. Labels 5 and 6 that are not correlated to the general trend are removed of the database for the calculation of the cumulative probability. Labels 11, 12 and 14 correspond to faults which damage zones were located on U.B.I. images. Label 11 corresponds to the littlest faults and Label 12 to the medium one in term of fracture sizes. Label 14 corresponds to the main fault of the Soultz reservoir.

The general trend observed on Figure 4 is not adapted to describe fracture labels 5 and 6 that represent continuous or wide open fractures on U.B.I. images. These fractures are not sufficiently numerous to fit with the general trend. One possible explanation could be that in this study only open fractures were taken into account. Indeed, a lot of same types of fractures are today totally sealed by sequences of

hydrothermal alteration. These sealed fractures were generated in the same time than those described by labels 5 and 6 and today still open. The paleo-fractures present similar widths than the still open ones but sealed widths. These wide open and continuous open fractures are the main fractures that could be percolated within the rock mass insuring the pervasive alteration of the granite when big faults generate more localized vein alteration (Sausse and Genter, 2006). A first explanation of this underestimation of the number of fracture labels 5 and 6 could therefore be that the missing fractures labels 5 and 6 are now sealed and therefore not take into account in the database.

Fracture labels 1, 2 and 3 are merged in one single group in the plot of Figure 4 because of the huge proportion of labels 1 in the database that mask the influence of 50% and 75% continuous fracture traces. This distinction is therefore not discriminant in this study.

A low fractal dimension such as 1.04 indicates that fractures are strongly clustered. This organization of very dense zones of fractures around the main fault corridors is well known at Soultz (Sausse and Genter, 2006).

### Cumulative number of fractures versus width

Harris et al. (1991) proposed to plot the cumulative number of fractures  $N_s$  as a function of their mean spacing  $S$  in a bi-logarithmic diagram, where  $N_s$  is the number of fracture spacing values higher than a specific spacing  $S$  (Figure 5).

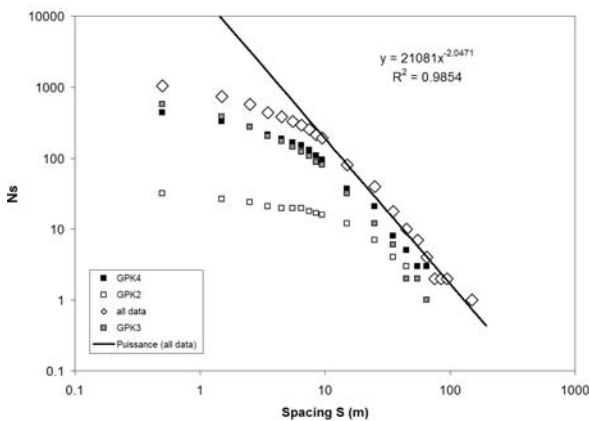


**Figure 5: Bi-logarithmic diagram of the cumulative number of fractures  $N_s$  as a function of their spacing  $S$ . The line is the best-fit curve of the whole fracture database spacings. The power law follows the equation  $N_s \sim S^{-(D+1)}$  where  $D$  is the fractal dimension characterizing the fracture set.**

The spacing  $S$  is the mean distance along the well path between one fracture and fractures  $i-1$  and  $i+1$ . This methodology has been applied for each Soultz deep wells GPK2, GPK3 and GPK4 and the three resulting plots were compared. Harris et al. (1991) proposed a relation between  $N_s$  and  $S$  following the equation:

$$N_s \approx S^{-(D+1)} \quad (3)$$

where  $D$  is the fractal dimension of the fractures set. The best-fit curve following equation 3 is quite difficult to determine in this case because of the dispersion of  $N_s$  and  $S$ . However, a same fractal dimension  $D$  equal to 1.04 is obtained and corresponds to a slope  $s$  of the curve equal to -2.04. A value of  $D$  of  $1.04 \pm 0.1$ , i.e.  $D$  in  $[1;1.1]$  seemed to

be well adapted to describe the spacing data ( $R=0.8701$ ) of the three Soultz wells.

### 3.3.2 Extension of the fractures

Determining the extension of a fracture is the main source of uncertainty in the hydraulic models. In fact, there is no consensus between authors concerning the best and most relevant method.

Gudmundsson (2000) made observations at reservoir scale concerning the length of veins observed in flow lavas. He determined that there is a linear relationship between the extension of a fracture  $L$  and its width  $W$  of a fracture of the form:

$$L = k \cdot W \quad (5)$$

where  $k$  is a coefficient characteristic of the facies. In the case of the veins observed in flow lavas,  $k$  is equal to 400 but with a poor correlation factor,  $R = 0.81$ .

Vermilye and Scholz (1995) state the same observations on fractures in different magmatic and sedimentary facies. In the case of the granodiorite of the Florence Lake, quite similar to the monzogranite of Soultz (porphyritic granite), the coefficient  $k$  is equal to 526 with a good correlation factor,  $R^2 = 0.96$  (42 measures ranging in extension from 23 mm to 23.7 m, in width from 0.1 mm to 4.5 mm). However, the authors notice that the correlation factors are sometimes very bad for a linear regression ( $R^2 = 0.28$  in limestones,  $R^2 = 0.22$  in argilites,  $R^2 = 0.66$  in sandstones).

Johnston and Mc Caffray (1996) proposes another relation between width and extension. Collecting data for five study areas with widely varying structural geometries in a variety of host rock types, they determine that the extension and the width of a fracture are proportional in some cases but that they follow a more generalized power-law of the form:

$$L = k \cdot W^d \quad (6)$$

where  $k$  is a coefficient characteristic of the facies ranging from 20 to 2000 for granitic facies, and  $D$  the fractal dimension of the fracture set. The coefficient  $k$  is higher in extensional context than in compression one, ranging from 57 to 1231 with a mean value of 402.

We decided then to follow the hypothesis of Johnston and Mc Caffrey (1996) and we chose to calculate the mean extension of the different labels using values of  $k = 400$  and  $D = 1.04$ . The results are reported in the following table:

Label & fracture type	Mean widths $W$ (cm)	Mean extensions $L$ (m)
1 Discontinuous open traces (25%)	3.15	11
2 Discontinuous open traces (50%)		
3 Discontinuous open traces (75%)		
4 Vuggy Fractures	10.69	39
5 Continuous open fractures	6.32	23
6 Wide open fractures	20.31	76
11 minor faults	150.11	610
12 medium faults	269.83	1123
14 major faults	626.53	2697

**Table 2: mean fracture extension by fracture labels**

The width of the damage zone associated to the major fault at Soultz is equal to 13 m. By application of the previous formula, its extension is therefore equal to 2.7 km which could be a correct estimation because this fault crosses the three wells on a minimum distance of 2 km.

## 4. MODELING OF THE FRACTURES SET

### 4.1 Density of fractures

To obtain the volumetric density of fractures, in number of fractures/m<sup>3</sup>, a method described by Chilès (personal communication), inspired by the work of Fouché and Diebolt (2004) was applied. First of all, the length  $L$  of the window in which we calculate the density is determined. A length  $L = 30\text{ m}$  (resolution of the final VOI grid) is fixed. This window length is then moved along the wells meter by meter. For each window, the number of fractures  $n$  that cross the well is determined. Then, for each window, the surface density  $\tilde{A}_v$  which is the ratio between the surface of fractures that cross the well in the window by the volume of the window is calculated. The assumption ( $H$ ) that each fracture  $i$  fully contributes to the 3D density measured is proposed. After simplification, the surface density becomes equivalent to equation 7:

$$\tilde{A}_v = \frac{1}{L} \cdot \sum_{i=1}^n \frac{1}{\cos \theta_i} \quad (7)$$

where  $\theta_i$  is the true dip of the fracture  $i$ .

This value of the surface density is overestimated because of the assumption ( $H$ ). Fouché and Diebolt (2004) propose the following correction parameter  $F_n$  which takes into account the Terzaghi correction for 2-D studies. The true surface density  $A_v$  is then:

$$A_v = F_n \cdot \tilde{A}_v \quad (8)$$

$$\text{With } F_n = \frac{n^2}{\sum_{i=1}^n \cos \theta_i \cdot \sum_{i=1}^n \frac{1}{\cos \theta_i}} \quad (9)$$

The next step consists to determine the mean surface of a fracture in the window. The results of the statistical analysis that determinate the extension of each fracture  $L$  in function of its width  $W$  ( $L = k \cdot W^D$ ) with  $k = 400$  and  $D = 1.04$  are used. Fractures are described by disks, which surface is equal to  $\pi(L/2)^2$ . Finally, the volumetric density of fractures in fractures/m<sup>3</sup> is obtained dividing  $A_v$  by  $S$ . This method was applied to the three wells GPK2, GPK3 and GPK4 and the volumetric density was reported in Figure 7 using a true vertical depth reference (T.V.D.S.S.). For each well, the density is plot. The matching between the depth location of the main faults that cross the wells and their associated damage zones is superimposed for GPK3 as an example.

The well GPK3 is the most fractured, with a mean density of 0.0056 fractures/m<sup>3</sup> (GPK2: 0.0015 fractures/m<sup>3</sup>; GPK4: 0.0052 fractures/m<sup>3</sup>). The well GPK4 is slightly less fractured than GPK3 but the difference between these two wells comes from the distribution of fracture length. GPK4 shows lowest fracture extensions despite this quite similar volumetric density that could explain its bad connectivity within the geothermic triplet.

Moreover, the influence of the faults and the extension of the damage zone can be observed clearly in Figure 7. The density of fractures around the main faults (ZF, Labels 11, 12 and 14 on Figure 7) is systematically and artificially low on U.B.I. images because of the impossibility of practical fracture picking in the damage zones that show too much density of thin fractures to clearly discern them. Grey zones on Figure 7 illustrate the density distribution around the main faults. The density peaks are symmetrical from fault

walls and allow to define a fault "zone of influence" around their characteristic depth. This "zone of influence" is estimated for the biggest fault zone (ZF-GPK3 Label 14 on figure 7) at 200 m wide above and below the main fault core. Other zones of influence could be clearly defined showing lowest amplitude than this last one.

Some correlation of density peaks could be too observed and must be now checked more precisely with the main fault orientations.

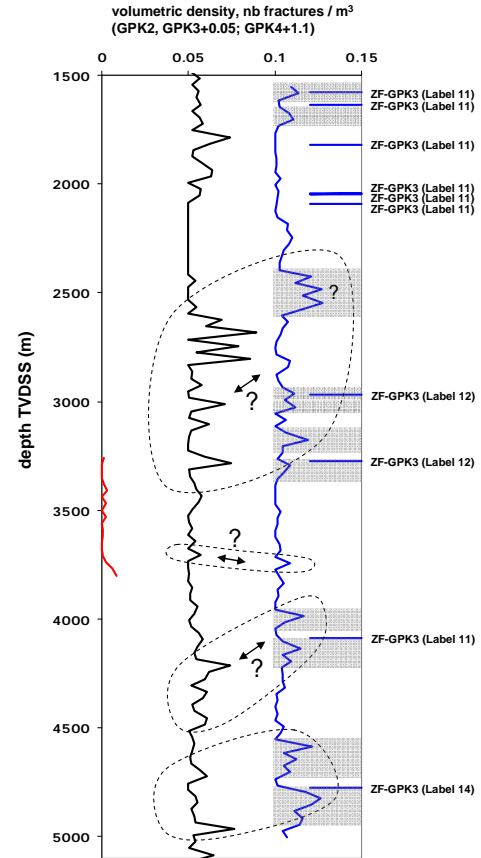


**Figure 7: Volumetric density at the wells GPK2, GPK3 and GPK4. The curves corresponding to the wells GPK3 and GPK2 are shifted by addition of 0.1 to the density of GPK3, 0.2 to the density of GPK4.**

### 4.2 Stochastic modeling

The statistical analysis and the calculation of the volumetric density for each well allow the initiation of the simulation process of a first DFN model. A D.F.N. process generates fractures as points distributed in the reservoir using a Poisson point process. Each fracture is characterized by its center and two vectors: its orientation (dip direction and dip) and its extension. These parameters are defined by distribution laws whose characteristics are defined by the previous statistical analysis. Thus, the distribution of the extension is not gaussian but follows a power-law distribution previously determined. The extension is defined respecting equation 6:  $L = k W^D$  and the fracture occurrence is defined respecting equation 2:  $P = k' W^{-D}$

The fracture extension distribution follows a power-law distribution and is the same that those observed for the different fracture labels. The dip directions and dips follow gaussian distributions that are defined for each facies and fracture sets using mean values and standard deviations / Fisher coefficients. The parameters extensions, dip

directions and dips are assigned to the simulated points by Monte-Carlo process.

The preliminary results of such D.F.N are now in progress. The difference of fracture density between the two granite facies is respected and the difference of fracturing is visible. Such type of D.F.N. allows to calculate the equivalent porosity and permeability properties in the VOI grid. First results give mean values of porosity around 5% and permeability around 25 milliDarcy in the reservoir. These first results must no be matched with the characteristic flow logs obtained since 2000 for GPK2, GPK3 and GPK4.

## 5. CONCLUSIONS

A new statistical analysis of the fault and fracture networks of the Soultz reservoir precises and finalizes the structural model of the reservoir. The statistical characterization of the fractures using U.B.I. images allow to define 1800 fractures along the three deep Soultz well paths, grouped into main conjugates fractures sets, showing a mean N.-S. orientation and a mean dip of 70°. Power-law type correlations between the geometric parameters of fractures, aperture, width and size are determined and a final fractal dimension D characterizing the fracture set is proposed. These parameters are used to determinate the volumetric density of fractures at the well scales and then within the gridded reservoir. Finally, the results of statistical analysis are used to perform stochastic simulation of a Discrete Fracture Network (D.F.N.). The comparison between D.F.N. models of the reservoir and flow test needs to be now discussed to define the uncertainties concerning the adjustment of the density maps, the influence of the various parameters (extensions, orientation distributions, etc.) and their impact on the hydraulic modeling of the reservoir.

## REFERENCES

- Bonnet E., Bour O., Odling N., Davy P., Main I., Cowie P., and Berkowitz B.: Scaling of fracture systems in geological media. *Geophysics*, **39**, (2001), 347-383.
- Dezayes C., Chevremont P., Tourliere B., Homeier G., and G. André.: Geological study of the GPK4 HFR borehole and correlation with the GPK3 borehole (Soultz-Sous-Forêts, France). *Technical Report RP-53697-FR*, BRGM, France, (2005).
- Dezayes C., Genter A., and Valley. B.: Structure of the low permeable naturally fractured geothermal reservoir at Soultz. *Geosciences*, (in press), (2009).
- Fouché O., and Diebolt J.: Describing the geometry of 3D fractures systems by correcting for linear sampling bias. *Mathematical Geology*, **36**, (2004), 33-63.
- Genter A. Géothermie Roches Chaudes Sèches : le granite de Soultz-Sous-Forêts (Bas Rhin, France). Fracturation naturelle, altérations hydrothermales et interactions eau-roche. *PhD thesis*, Orléans University, BRGM, (1989), 201 p.
- Genter A., Traineau H., Ledésert B., Bourguine B., and Gentier S.: Over 10 years of geological investigations within the HDR Soultz project, France. *Proceedings, World Geothermal Congress 2000, Kyushu-Tohoku*, Japan, May 28 - June 10 (2000).
- Gerard A., Genter A., Kohl T., Lutz P., Rose P., and Rummel F.: The deep EGS (Enhanced Geothermal System) project at Soultz-Sous-Forêts (Alsace, France). *Geothermics*, **35**, (2006), 473-483.
- Gudmundsson A.: Fracture dimensions, displacements and fluid transport. *Journal of Structural Geology*, **22** (2000), 1221-1331.
- Harris C., Franssen, R., and Loosveld R.: Fractal analysis of fractures in rocks : the Cantor's dust method - comment. *Tectonophysics*, **198** (1991), 107-115.
- Johnston J.-D., and Mc Cafrey K.: Fractal geometries of vein systems and the variation of scaling relationships with mechanism. *Journal of Structural Geology*, **18**, (1996), 349-358.
- Kim Y., Peacock D., and Sanderson D.: Fault damage zones. *Journal of Structural Geology*, **26** (2004), 503-517.
- Mandelbrot B.: Les objets fractals, forme, hasard et dimension. Nouvelle Bibliothèque Scientifique, 2<sup>nd</sup> édition, Flammarion, Paris, (1984).
- Nami P., Schellschmidt R., Schindler M., and Tischner T.: Chemical Stimulation Operations for Reservoir Development of the Deep Crystalline HDR/EGS System at Soultz-Sous-Forêts (France). *Proceedings, 33rd Workshop on Geothermal Reservoir Engineering, Stanford University*, Stanford, California, January 28-30 (2008).
- Sausse J., and Genter A.: Types of permeable fractures in granites. *Special publication of the Geological Society of London* (Harvey P.K., Brewer T.S., Pezard P.A. and Petrov V.A. (editors), **240** (2006), 1-14.
- Sausse J., Dezayes C., Dorbath L., Genter A., and Place J.: 3D model of fracture zones at Soultz based on geological data, image logs, induced microseismicity and vertical seismic profiles. *Geosciences*, (in press), (2009).
- Schindler M., Nami P., Schellschmidt R., Teza D., and Tischner T.: Review of Hydraulic Stimulation Operations in the 5 km Deep Crystalline HDR/EGS-Reservoir at Soultz-sous-Forêts. *Proceedings, 33rd Workshop on Geothermal Reservoir Engineering, Stanford University*, Stanford, California, January 28-30 (2008).
- Vermilye J., and Scholz C.: Relation between vein length and aperture. *Journal of Structural Geology*, **17**, (1995), 423-434.